JST: Engineering and Technology for Sustainable Development
Volume 34, Issue 3, July 2024, 001-007

Adsorptive Removal and Photo-Fenton Degradation of Congo Red Dye from Water Using Modified Gadolinium Orthoferrite

Thi To Nga Phan*, Thi Thu Huyen Nguyen
School of Chemistry and Life Sciences, Hanoi University of Science and Technology, Ha Noi, Vietnam
**Corresponding author email: nga.phanthito@hust.edu.vn*

Abstract

$GdFeO_3$-incoporated zeolite (GFO/Z) was successfully prepared by the impregnation method followed by the calcination process and used for adsorption and photo-Fenton degradation of Congo Red (CR). The as-prepared GFO/Z material was characterized by X-ray Diffraction (XRD), scanning electron microscopy (SEM), transmission electron microscopy (TEM), Brunauer–Emmett–Teller (BET) surface area, and optical absorption spectra (UV-Vis). The large specific surface area and accessible pores supported its high performance towards the adsorption of CR . Besides, due to its low band gap energy, the photo-Fenton catalytic activities of GFO/Z were also investigated for the degradation of CR under visible light irradiation. The use of GFO/Z led to a high removal rate (97.46%) of CR thanks to the synergistic effect between effective dark adsorption and visible-light-driven Fenton degradation, which was greater than those of pure GFO. Scavenger experiments were performed to reveal that the hydroxyl radicals (•OH) were the main active species in the photo-Fenton catalytic process. This work showed a promising application of GFO/Z in the degradation of organic compounds in wastewater.

Keywords: $GdFeO_3$, zeolite, impregnation method, adsorption, photo-Fenton, CR.

1. Introduction

Synthetic dyes are one of the most common contaminants that are found in contaminated wastewater from many industries such as textiles, plastics, paper, rubber, etc. [1]. Most dyes can result in damage not only to aquatic systems but also to human well-being due to their toxic, carcinogenic, and mutagenic [2]. CR [1-naphthalene sulfonic acid,3,3'-(4,4'-biphenylenebis (azo)) bis (4-amino-) disodium salt] is a benzidine-based dye, exhibiting difficulty in biodegradation due to its structural stability [3]. This dye can be metabolized to benzidine, which is known as a human carcinogen. From an environmental point of view, it is necessary to remove the dyes before discharging them into the environment. However, the high stability and resistance to light and oxidizing agents are major obstacles in the treatment of dye-containing wastewater. So far, a number of techniques have been developed and used for the removal of dye-containing effluents, including coagulation/flocculation, ozonation, advanced oxidation processes (AOPs), membrane filtration, adsorption, and biological treatment.

Of these methods, the combination between adsorption and photodegradation (one of the AOPs) is recognized as a promising and attractive alternative because of its high efficiency, simplicity and availability of a wide range of adsorbents and photocatalysts [4, 5]. A large number of adsorbents such as clay minerals, bentonite, fly ash, rice husk, and fungi have been treated for CR removal, but their effectiveness is limited. Therefore, it is significant and necessary to search for more effective adsorbents.

$GdFeO_3$ (GFO), one type of perovskite oxides, has been widely utilized in fuel cells, photocatalyst, and sensors, and has attracted great scientific interest. Although GFO has been proven in theoretical studies to be effective in the adsorption of some molecules [6, 7], experimental work on the adsorptive removal of organics by GFO is hardly reported. In addition, similar to other perovskites, its use is limited due to the relatively small specific surface area of particles, which results in low accessibility of pollutants to the active sites and in turn may affect adsorptive removal capacity. In order to overcome this limitation, a series of outstanding attempts have been carried out to load perovskite crystals to different types of porous materials, including silica, carbon, montmorillonite, and zeolite. Among them, the supports of zeolite show a number of advantageous features, i.e. high pore volume, large surface area, and uniform pore structure [8].

Until now, there has been some progress in reporting the utilization of metal/metal oxide-supported zeolite as adsorbent materials or photocatalysts to remove CR from water [9, 10]. For

ISSN 2734-9381
https://doi.org/10.51316/jst.175.etsd.2024.34.3.1
Received: Mar 10, 2024; revised: Apr 25, 2024;
accepted: May 27, 2024

example, the adsorption of ZnO/zeolite reached 161.3 mg/g at 0.05 g/l of solid dosage, pH 3 and CR concentration of 100 mg/l [9]. The material of Cu-impregnated zeolite Y showed a goodphoto-Fenton degradation of CR with 95.34% after 2 h exposure to visible light irradiation [10].

However, there is a lack of information on the synergistic effect of adsorption and photodegradation process and especially the optimization of favorable conditions in the adsorptive removal of CR over perovskite materials. Therefore, herein we reported the synthesis of GFO-impregnated zeolite and its application as an adsorbent and photocatalyst for CR removal from water. The adsorption behavior and photo-Fenton degradation of CR were investigated in detail. To the best of our knowledge, there has been no such work published in literature.

2. Materials and Methods

2.1. Materials

Gadolinium nitrate hexahydrate ($Gd(NO_3)_3{\cdot}6H_2O$; 99.9%), Iron nitrate nonahydrate ($Fe(NO_3)_3{\cdot}9H_2O$; 98%), citric acid ($C_6H_8O_7{\cdot}H_2O$; ≥99.5%), CR ($C_{32}H_{22}N_6Na_2O_6S_2$, 97%), hydrogen peroxide solution (H_2O_2, 30%), and ammonium hydroxide solution (NH_4OH, 30%) were purchased from Sigma-Aldrich. Zeolite was a product from Zeolite Australia Limited Company, Australia. All chemicals were of analytical grade and used as received without further purification.

2.2. Synthesis of $GdFeO_3$-Doped Zeolite

$GdFeO_3$-doped Zeolite (GFO/Z) was synthesized by the impregnation method, followed by the calcination process. Typically, 0.005 mol $Gd(NO_3)_3.6H_2O$, 0.005 mol $Fe(NO_3)_3.9H_2O$, and 0.01 mol citric acid were dispersed in a solution of 15 mL distilled water and ethanol. The mixture was stirred for 3 h, followed by adding 1 g of zeolite. The resulting solution was kept continuously stirring at 70 °C for 2 h and then drying at 80 °C overnight. The obtained GFO/Z was collected after calcining at 700 °C for 4 h (at a heating rate of 2 ºC/min). Pure GFO was prepared *via* a similar procedure as above without adding zeolite and used to compare with GFO/Z in the adsorptive removal and photodegradation of CR.

2.3. Characterizations of Photocatalyst

The characterizations of the samples were examined by using modern techniques as follows. X-ray diffraction (XRD) patterns were performed on a D8 Advance-Bruker diffractometer using Cu Kα radiation ranging from 10° to 80°. The morphology was characterized by using a Zeiss-1555 scanning electron microscopy (SEM) at an accelerating voltage of 5 kV. Transmission electron microscopy (TEM) images were recorded on a TEM-TITAN operating at 200 kV. The surface area and pore size were obtained from the nitrogen adsorption-desorption at 77 K on SAPA2010 (Micromeritics Inc., USA). UV-vis absorption spectra of the samples were examined by UV vis-DRS-Agilent 8453 spectrophotometer.

2.4. Removal of CR by Adsorption and Photo-Fenton Degradation Processes

2.4.1. CR adsorption test

In the CR adsorption test, a polypropylene bottle containing 200 mL of 50 mg/l CR solution with 200 mg of GFO/Z was used. The sealed bottle was kept in the shaker bath to achieve equilibrium at 25 °C. A small amount of suspension was withdrawn and centrifuged at a given time during the adsorption. The concentration of CR was confirmed by using the UV/Vis spectrophotometer (UVmini-1204, Shimadzu, Japan). The amount of CR adsorbed on GFO/Z at time t (q_t (mg/g)) was calculated as follows:

$$q_t = \frac{(C_0 - C_t)V}{m} \quad (1)$$

where C_0 and C_t are the CR concentrations at initial time and at time *t* (mg/l), respectively; *V* is the volume of solution (L) and *m* is the mass of GFO/Z (g).

2.4.2. Photo-Fenton degradation test of CR

100 mg GFO/Z was dispersed in 100 mL solution of 50 mg/l CR. A 300W Xenon lamp (CEL-HX 300) with a 400 nm cut-off filter was used as a visible light irradiation source. Prior to starting visible light irradiation, the suspension was magnetically stirred in the dark for 120 min to achieve the adsorption–desorption equilibrium of CR on GFO/Z. The photo-Fenton reaction starts after adding H_2O_2 and turning on the visible light source, which lasts for 120 min. In order to determine the CR concentration, a small amount of sample was taken out from the suspension every 10 mins and then analyzed using a UV/Vis spectrophotometer.

The removal rate was calculated as follows:

$$\text{Removal rate (\%)} = \frac{(C_1 - C_t)}{C_1} \times 100\% \quad (2)$$

where C_1 and C_t (mg/l) are the CR concentrations at the initial time (after finishing adsorption process) and at time *t* during photo-Fenton degradation test, respectively.

3. Results and Discussion

3.1. Characterizations

Fig. 1 shows the XRD patterns of GFO/Z in comparison with that of GFO and Z. The reflection peaks of Z are consistent with the literature [11], as shown in Fig. 1. Moreover, after GFO was integrated into Z *via* the impregnation – calcination process, the main characteristic peak of Z at 26.6º was retained.

Noting that the intensity of this characteristic peak in the GFO/Z sample was slightly lower than that of Z, which could be attributed to the introduction of GFO crystalline particles. Meanwhile, XRD pattern of GFO/Z still appeared several peaks at 2θ of 32.1, 39.1, 47.4 and 59.6°, which are identical to those in the XRD pattern of orthorhombic GFO (JCPDS no. 47-0067) [12]. The density of GFO characteristic peaks in GFO/Z sample was found to be lower. This implies the successful cooperation of GFO crystals onto the Z support. No other impurity diffraction peaks are observed in Fig. 1, confirming the high purity of GFO/Z sample.

Fig. 2a and b present the SEM images of Z and GFO-integrated Z samples. Z was observed as the agglomerated particles with irregular shapes in a layered-like structure (Fig. 2a). Meanwhile, the SEM observation of GFO/Z in Fig. 2b shows a similar morphology. This suggests that doping with GFO on to Z support did not considerably influence the morphology of Z support. The TEM image of GFO/Z in Fig. 2c demonstrates the dark spots, referring to dispersed GFO nanoparticles distributed in the Z support.

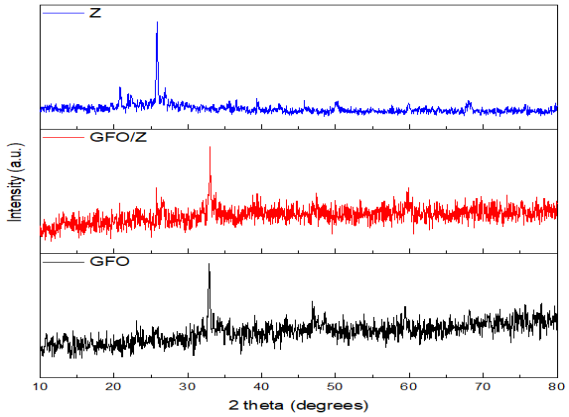

Fig. 1. XRD patterns of Z, GFO and GFO/Z

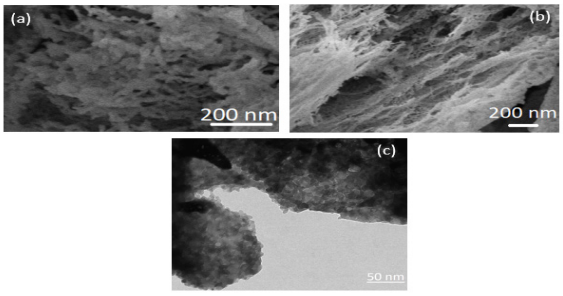

Fig. 2. SEM images of (a) GFO and (b) GFO/Z and TEM image of GFO/Z (c)

Table 1. Structural property of the samples

Sample	S_{BET} (m^2/g)	Pore volume (cm^3/g)	Average pore size (Å)
GFO	7.33	0.062	35.96
Z	52.06	0.163	87.91
GFO/Z	20.71	0.102	98.34

The textual properties, including BET specific surface area, pore volume and average pore size of GFO, Z, and GFO/Z are listed in Table 1. There was a gradual loss of BET specific surface area of Z from 52.06 m^2/g to 20.71 m^2/g in GFO/Z sample after the incorporation of GFO in Z. This might be ascribed to the impregnation and dispersion of GFO in the cavities and channels Z support. Moreover, the decrease in total pore volume of GFO/Z further suggests the successful integration of GFO into the channels of GFO/Z, which are expected to be the active sites for CR degradation.

It is well known that one of the most important factors in determining a material's photocatalytic activity is its energy band structure. Fig. 3a illustrates the UV–vis absorption spectra of the three samples Z, GFO, and GFO/Z. As can be seen clearly from Fig. 3a, two samples GFO and GFO/Z prepared from the impregnation method showed similar optical absorption abilities. The absorption spectra exhibited an absorption in UV region (at around 320 nm) and over visible light to near IR region (400 nm –800 nm). Meanwhile, Z sample showed no absorption capability in visible region.

The optical band gap of these samples can be calculated based on the reflectance spectral data following the Kubelka-Munk equation [13]:

$$F(R) = \frac{(1-R)^2}{2R} \quad (3)$$

where $F(R)$ is Kubelka-Munk function and R is reflectance. The relationship between $[(F(R).hv)^2]$ and hν in the allowed direct electron transition is shown in the inset of Fig. 3b. In Fig. 3b, the band gap values of GFO/Z sample were found to be 2.78 eV, which was narrower than that of GFO (2.98 eV). Obviously, the incorporation of GFO onto Z support improved the light absorption ability of GFO/Z sample. This suggests their suitability for photocatalytic degradation of organic compounds under activation by visible light irradiation.

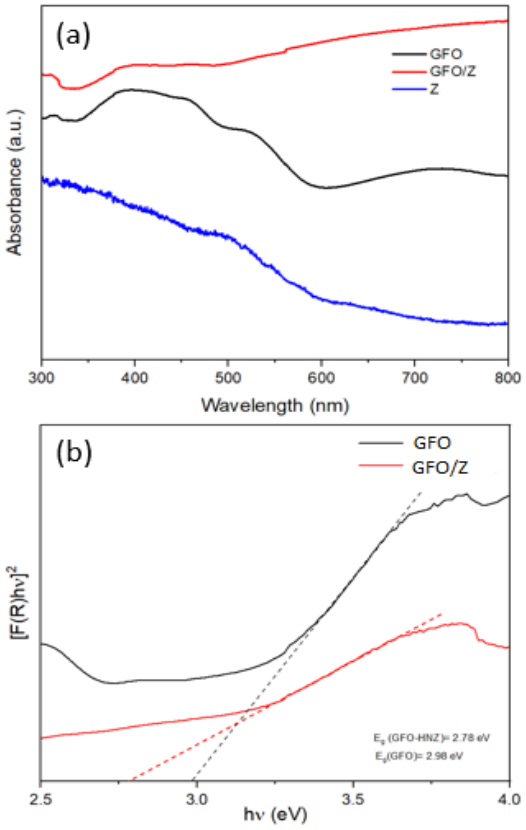

Fig. 3. (a) UV-Vis absorption spectra of the samples and (b) plot of $(F(R)h\nu)^2$ versus $h\nu$

3.2. Removal of CR by Adsorption Process

Fig. 4 shows the effect of integrating GFO on zeolite support on CR adsorption in comparison with the pure GFO and zeolite samples. As can be seen from Fig. 4, after reaching equilibrium, the absorption capacity of zeolite for CR showed a relatively low value of 3.44 mg/g. Meanwhile, the equilibrium adsorption capability of GFO was 12.43 mg/g, which can be ascribed to the complex that formed between Gd, Fe, and CR.

It is worth noting that, GFO/Z sample illustrated improved adsorption ability for CR with adsorption amount of (34.03 mg/g), implying that the GFO particles are the adsorption sites for CR. Indeed, the adsorption process of CR by GFO/Z took place thanks to the good accessibility of CR into the pores of GFO/Z. Moreover, the GFO species which were cooperated inside the pores of zeolite were also considered as the active sites for CR adsorption. Therefore, the adsorbent of GFO/Z exhibited a higher adsorption amount of CR than the pure GFO and zeolite at equilibration time. The adsorption ability of other ferrite perovskites for CR presented a similar trend to GFO/Z [14, 15]. This study mentioned that the adsorption capability of adsorbents mainly depended on the distribution of Fe species and various complexation types between adsorbent and anionic pollutants.

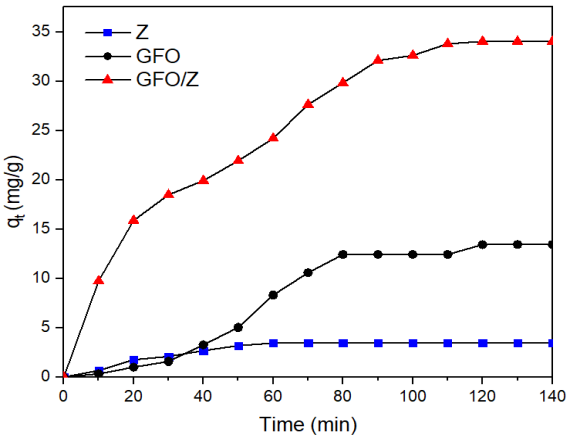

Fig. 4. Effect of different adsorbents on the removal of CR (conditions: temperature = 25 °C; adsorbent dosage = 1 g/l; CR concentration = 50 mg/l; pH 5)

3.3. Photo-Fenton Degradation of CR

The photo-Fenton degradation activities of GFO and GFO/Z were evaluated by the degradation of CR under visible light irradiation in the presence of H_2O_2. Before starting visible light irradiation, the adsorption of CR onto GFO and GFO/Z was finished with the CR removal of 25.16 and 68.86%, respectively. As shown in Fig. 5, the GFO/Z sample demonstrated a good performance toward CR degradation under visible light irradiation, which was 97.46% of CR removed after 120 min. This is obviously higher than 37.43% of CR removed by GFO.

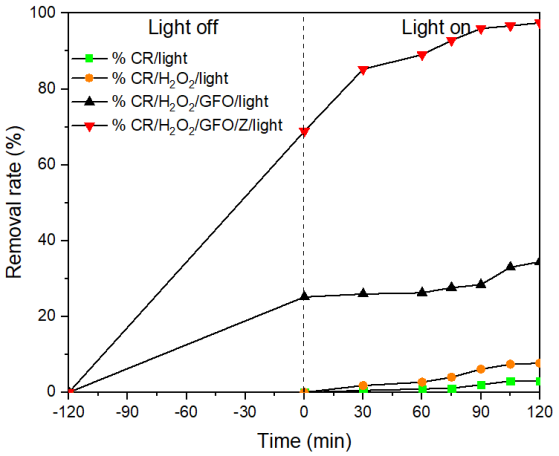

Fig. 5. Removal of CR during adsorption and photo-Fenton degradation processes using GFO and GFO/Z (conditions: temperature = 25 °C; CR concentration = 50 mg/l; catalyst dosage = 1g/l; H_2O_2 concentration = 10 mM; pH 5)

Meanwhile, during self-photolysis process, CR was degraded 3% only and the removal rate was slightly improved up to 7.7% when adding H_2O_2 (Fig. 4a). It is worth noting that CR itself was hardly decomposed by visible light or H_2O_2 while a greater

CR degradation rate was obtained when both GFO/Z and H_2O_2 were present under visible light illumination. This implies that GFO/Z could act as a heterogeneous catalyst for the photo-Fenton degradation of CR in the visible region.

In comparison with another perovskite/porous support [16], the photo-Fenton degradation of CR by our GFO/Z was promising (noting that the reaction conditions varied). In particular, GFO/Z removed 97.46% CR after 90 min exposure to visible light irradiation (reaction conditions: dye concentration = 50 mg/L; catalyst dosage = 1.0 g/l; H_2O_2 concentration = 10 mM; solution pH = 5, and temperature = 25 °C). Meanwhile, the $BiFeO_3$ supported graphene only degraded 62% CR after 120 min visible light irradiation (reaction conditions: dye concentration = 100 mg/L; catalyst dosage = 1.0 g/L) [16].

In order to clarify the reaction kinetic of CR degradation, the pseudo-first-order model was used:

$$-ln\frac{(C_t)}{C_1} = kt \quad (4)$$

where C_1 and C_t are the CR concentrations before the photo-Fenton degradation and after time t in the photo-Fenton reaction, respectively; k is the pseudo-first-order rate constant.

The rate constant *(k)* was calculated from the slope of plot of -ln (C_t/C_1) versus time in Fig. 6. At optimized conditions, the first order kinetic constant k of GFO/Z was 0.0323 min^{-1}, which was about 10 times than that of pure GFO. The higher k value implies a faster degradation rate and higher photo-Fenton catalytic efficiency. It should be noted that the porosity characteristic of GFO/Z sample may be responsible for its higher adsorption capacity and in turn, improving the photo-Fenton degradation efficiency. Obviously, the adsorption of CR over GFO/Z was considerable in Fig. 5 compared to that of the pure GFO sample.

In order to clarify the role of reactive species for photo-Fenton degradation of CR using GFO/Z sample, the trapping experiments were performed to investigate the effect of active species hydroxyl radicals (•OH)) and holes (h^+) on the photo-Fenton degradation process. Isopropanol (IPA, Sigma Aldrich) and Ethylenediaminetetraacetic acid (EDTA, Sigma Aldrich) were used as •OH and h^+ scavengers, respectively, as shown in Fig. 7.

Fig. 7 showed the CR photo-Fenton degradation rate by GFO/Z only (no scavenger) and in the presence of the scavengers. As can be seen from Fig. 7, there was no significant change in the photo-Fenton degradation rate when introducing EDTA in the reaction solution, suggesting that the role of holes in the photo-Fenton catalytic degradation of CR is relatively minor. Meanwhile, when adding IPA, a significant suppressed degradation rate was observed, which implied that the hydroxyl radicals •OH play an important role in the CR photo-Fenton degradation. This observation is consistent with what had been reported in previous studies [17, 18].

The following is a potential photo-Fenton catalytic mechanism utilizing GFO/Z that was suggested based on the aforementioned results. It is well known that the GFO/Z photocatalyst's interfacial Fe atoms (designated as Fe^{3+}) can combine with H_2O_2 during a Fenton-like reaction to produce •OH radicals according to the following equation. These radicals then directly oxidize CR to degradation products (equation (11)) [19]:

$$Fe^{3+} + H_2O_2 \rightarrow Fe^{3+} + H_2O_2 \quad (5)$$

$$Fe^{3+} + H_2O_2 \rightarrow Fe^{2+} + HO_2 + H^+ \quad (6)$$

$$Fe^{3+} + HO_2 + H^+ \rightarrow Fe^{2+} + O_2 + 2H^+ \quad (7)$$

$$Fe^{2+} + H_2O_2 \rightarrow Fe^{3+} + \bullet OH + OH^- \quad (8)$$

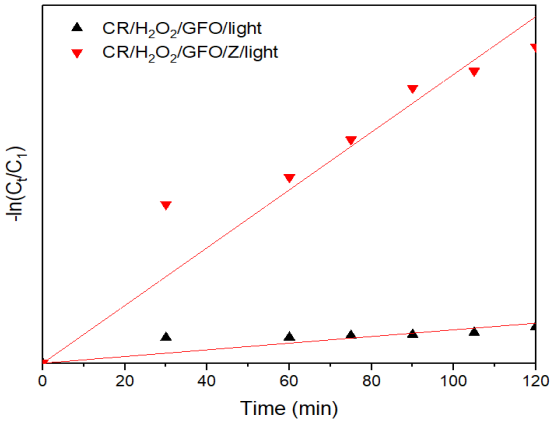

Fig. 6. Plots of -ln(C_t/C_1) *versus* irradiation time (conditions: temperature = 25 °C; CR concentration = 50 mg/l; catalyst dosage = 1g/l; H_2O_2 concentration = 10 mM; pH 5)

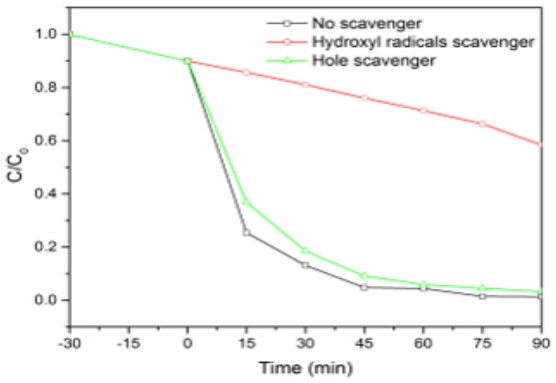

Fig. 7. Effect of IPA and EDTA on the photo-Fenton degradation of CR over GFO/Z (reaction conditions: photocatalyst dosage = 1g/L, H_2O_2 = 10 mM, CR concentration = 500 mg/L, pH 5)

The following equation describes how the GFO/Z photocatalyst experiences charge separation under visible light irradiation, producing electrons (e^-) and holes (h^+) concurrently:

$$GFO/Z + h\nu \rightarrow GFO/Z\ (e^- + h^+) \quad (9)$$

The electrons were then trapped by H_2O_2 to form the •OH which participated in the CR degradation reaction, as follows:

$$H_2O_2 + e^- \rightarrow \bullet OH + OH^- \quad (10)$$

$$\bullet OH + CR \rightarrow \text{Degradation products} \quad (11)$$

As a result, the combination of photocatalysis and heterogeneous Fenton-like reaction leads to an enhancement in the removal rate of CR.

3.4. Stability and Reusability of GFO/Z Photocatalyst

In terms of practical application, the stability and reusability of a photocatalyst is one of the important factors to evaluate its quality. Besides, photocatalysts are highly reusable and keep the majority of their activity even after multiple continuous cycles of use, which is necessary for the application of photo-Fenton. As can be seen from Fig. 8, the CR removal over GFO/Z gradually decreased during the tests, from 97.46% in the first cycle to 92.68% in the fourth run. This suggests that GFO/Z could be reused for four cycles without significant photocatalyst deactivation.

In addition, we studied the structure of GFO/Z sample after the fourth run of CR removal test. Fig. 9 demonstrated that the XRD pattern of spent GFO/Z remained unchanged in comparison with that of GFO/Z at the first run. This suggests that the GFO/Z can function as an effective photo-Fenton catalyst for the photo-Fenton degradation of organic pollutants under visible light irradiation with good stability.

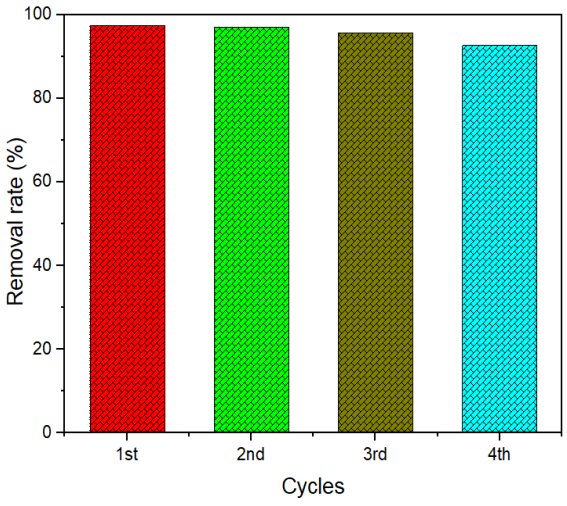

Fig. 8. CR removal over GFO/Z after four cycles

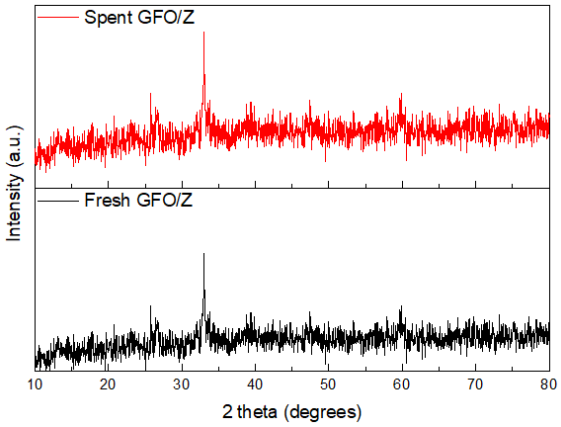

Fig. 9. XRD patterns of GFO/Z before and after adsorption and photo-Fenton degradation of CR

4. Conclusion

$GdFeO_3$ incorporated with zeolite (GFO/Z) has been successfully prepared by the impregnation method following by calcination process. The GFO/Z sample showed a synergistic effect of adsorption and the photo-Fenton process for the removal of CR, resulting in a total CR removal rate of 97.46% after 120 min, which is higher than that of pure GFO. The trapping experiment suggested that the hydroxyl radicals played the role of the active species in this reaction. The high removal efficiency of GFO/Z confirmed that it could be used as an effective heterogeneous photo-Fenton catalyst for the degradation of CR in aqueous media.

Acknowledgments

This research is funded by Vietnam National Foundation for Science and Technology Development (NAFOSTED) under grant number 104.05-2020.06.

References

[1] Ayele A., Getachew D., Kamaraj M., and Suresh A., Phycoremediation of synthetic dyes: an effective and eco-friendly algal technology for the dye abatement, J. Chem., vol 2021, Apr. 2021. https://doi.org/10.1155/2021/9923643

[2] Islam T., Repon MR., Islam T., Sarwar Z., and Rahman M., Impact of textile dyes on health and ecosystem: a review of structure, causes, and potential solutions, Environ. Sci. Pollut. Res., vol. 30, no.4, pp. 9207-9242, Dec. 2022. https://doi.org/10.1007/s11356-022-24398-3

[3] Al-Harby N. F., Albahly E. F., and Mohamed N. A., Synthesis and characterization of novel uracil-modified chitosan as a promising adsorbent for efficient removal of Congo red dye., Polymers, vol. 14, no. 2, pp. 271, Jan. 2022. https://doi.org/10.3390/polym14020271

[4] Chatterjee S.,Lee D. S., Lee M. W., and Woo S. H., Enhanced adsorption of congo red from aqueous solutions by chitosan hydrogel beads impregnated with

cetyl trimethyl ammonium bromide, Biores. Technol., vol. 100, no. 11, pp. 2803-2809, June. 2009. https://doi.org/10.1016/j.biortech.2008.12.035

[5] Han R., Ding D., Xu Y., Zou W., Wang Y., Li Y., and Zou L., Use of rice husk for the adsorption of congo red from aqueous solution in column mode, Biores. Technol., vol. 99, no. 8, pp. 2938-2946, May 2008. https://doi.org/10.1016/j.biortech.2007.06.027

[6] Kryuchkova T. A., Kost V. V., Sheshko T. F., Chislova I. V., Yafarova L. V., and Zvereva I. A., Effect of cobalt in $GdFeO_3$ catalyst systems on their activity in the dry reforming of methane to synthesis Gas, Petroleum Chem., vol. 60, pp. 609-615, May 2020. https://doi.org/10.1134/S0965544120050059

[7] Sheshko T. F., Sharaeva A. A., Powell O. K., Serov Y. M., Chislova I. V., Yafarova L. V., Koroleva A. V., and Zvereva I. A., Carbon oxide hydrogenation over $GdBO_3$ (B= Fe, Mn, Co) complex oxides: effect of carbon dioxide on product composition, Petroleum Chem., vol. 60, pp. 571-576, May 2020. https://doi.org/10.1134/S0965544120050114

[8] Hu G., Yang J., Duan X., Farnood R., Yang C., Yang J., Liu W., and Liu Q., Recent developments and challenges in zeolite-based composite photocatalysts for environmental applications, Chem. Eng. J., vol. 417, pp. 129209, Aug. 2021. https://doi.org/10.1016/j.cej.2021.129209

[9] Madan S., Shaw R., Tiwari S., and Tiwari S. K., Adsorption dynamics of Congo red dye removal using ZnO functionalized high silica zeolitic particles, Appl. Surf. Sci., vol. 487, pp. 907-917, Sep. 2019. https://doi.org/10.1016/j.apsusc.2019.04.273

[10] Singh L., Rekha P., and Chand S., Cu-impregnated zeolite Y as highly active and stable heterogeneous Fenton-like catalyst for degradation of Congo red dye, Sep. Purif. Technol., vol. 170, pp. 321-336, Oct. 2016. https://doi.org/10.1016/j.seppur.2016.06.059

[11] Saputra E., Budihardjo M. A., Bahri S., and Pinem J. A., Cobalt-exchanged natural zeolite catalysts for catalytic oxidation of phenolic contaminants in aqueous solutions, J. Water Process Eng., vol. 12, pp. 47-51, Aug. 2016. https://doi.org/10.1016/j.jwpe.2016.05.012

[12] Hui S., Jiayue X., and Anhua W., Preparation and characterization of perovskite $REFeO_3$ nanocrystalline powders, J. Rare earths, vol. 28, no. 3, pp. 416-419, June 2010. https://doi.org/10.1016/S1002-0721(09)60124-1

[13] Albadi Y., Ivanova M. S., Grunin L. Y., Martison K. D., Chebanenko M. I., Izotova S. G., Nevedomskiy V.N., Abiev R.S., and Popkov V.I., The influence of co-precipitation technique on the structure, morphology and dual-modal proton relaxivity of $GdFeO_3$ nanoparticles, Inorganics, vol. 2021, May 2021. https://doi.org/10.3390/inorganics9050039

[14] Santos A. G., Leite J. O., Gimenez I. F., Souza M. J. B., and Pedrosa A. M. G., Effect of the B-site cation from $LaBO_3$ and $LaBO_3/TiO_2$ (B= Mn or Ni) perovskites prepared by mechanosynthesis in adsorption of Congo red dye from aqueous medium, Mater. Res. Express, vol. 6, no. 10, pp. 105065, Aug. 2019. https://doi.org/10.1088/2053-1591/ab3b22

[15] Santos A. G., Leite J. O., Souza M. J. B., Gimenez I. F., and Pedrosa A. M. G., Effect of the metal type in perovskites prepared by modified proteic method in dye adsorption from aqueous medium, Ceram. Inter.l, vol. 44, no. 5, pp. 5743-5750, Apr. 2018. https://doi.org/10.1016/j.ceramint.2017.12.232

[16] Fatima S., Ali S. I., Iqbal M. Z., and Rizwan S., Congo red dye degradation by graphene nanoplatelets/doped bismuth ferrite nanoparticle hybrid catalysts under dark and light conditions, Catal.,vol. 10, no. 4, pp. 367, Mar. 2020. https://doi.org/10.3390/catal10040367

[17] Simsek E. B., Tuna O., and Balta Z., Construction of stable perovskite-type $LaFeO_3$ particles on polymeric resin with boosted photocatalytic Fenton-like decaffeination under solar irradiation, Sep. Purif. Technol., vol. 237, pp. 116384, Apr. 2020. https://doi.org/10.1016/j.seppur.2019.116384

[18] Balta Z., and Simsek E. B., Understanding the structural and photocatalytic effects of incorporation of hexagonal boron nitride whiskers into ferrite type perovskites ($BiFeO_3$, $MnFeO_3$) for effective removal of pharmaceuticals from real wastewater, J. Alloys Comp., vol. 898, pp. 162897, Mar. 2022. https://doi.org/10.1016/j.jallcom.2021.162897

[19] Anantharaman, A., Josephine B., Mary T. V., Ajeesha T. L., and Mary G., Photo-Fenton activity of magnesium substituted cerium ferrite perovskites for degradation of methylene blue via sol–gel method, J. Nanosci. Nanotechnol., vol. 19, no. 8, pp. 5116-5129, 2019. https://doi.org/10.1166/jnn.2019.16819